

Ultra-fine Ni₂P nanoparticles decorated r-GO: Novel Phosphidation approach and Dibenzothiophene Hydrodesulfurization

Vasileios Tzitzios^{*§, b}, Vishnu Pillai[‡], Christina Gioti[¶], Marios Katsiotis[£], Thomas Karagiannis[‡], Dimitrios Gournis[¶], Michael A Karakassides[¶] and Saeed Alhassan^{*‡}

[§] Institute of Nanoscience and Nanotechnology, NCSR “Demokritos” 15310, Athens, Greece

[‡] Department of Chemical Engineering, Khalifa University of Science and Technology, Petroleum Institute, P.O. Box 2533, Abu Dhabi, United Arab Emirates

[¶] Department of Materials Science and Engineering, University of Ioannina, 45110, Ioannina, Greece

[£] TITAN Cement Company S.A.

Abstract. Nanostructured transition metal phosphides gathered last years an elevated scientific interest, due to their unique physical-chemical properties. Nickel phosphide nanoparticles, with the controllable crystal structure, from the metal rich tetragonal Ni₁₂P₅ to the phosphorous rich hexagonal Ni₂P, and *hcp* Ni₂P decorated r-GO (reduced graphene oxide), nano-hybrid materials have been synthesized via a novel one step organometallic approach in primary-tertiary aliphatic amines mixture. The nanoparticles are monodispersed, with spherical shape and controllable size in the sub-10 nm regime and decorate uniformly the surface of the r-GO, leading to the formation of Ni₂P/r-GO hybrid materials. The materials were characterized by powder XRD, TEM and Raman spectroscopy and catalytically evaluated for the dibenzothiophene hydrodesulphurization (HDS) reaction. The results show that the role of the tertiary amine is crucial for the phosphidation process and the r-GO is an ideal alternative, to the traditional inorganic ones, support for the immobilization of the catalytically active component, preventing significantly sintering effects.

Keywords: *Ni₂P colloids, r-GO, composite nanomaterials, chemical synthesis, phosphidation reaction, hydrodesulphurization, dibenzothiophene*

INTRODUCTION

During last decades the extensive study of matter in the nanosize regime (<100 nm) have already gave an enormous boost in the materials science, introducing materials with improved or even novel physicochemical properties. Transition metal phosphides, although they discovered in the 18th century, in contrast with metallic, metal oxides and metal chalcogenide (quantum dots) nanoparticles, attract significant scientific interest in the last decades because of their potential applications, mainly in the fields of catalysis, replacing noble and precious metals, semiconductors and magnetic materials.¹⁻⁵

With respect to catalysis, transition metal phosphides are being evaluated as hydro-treating catalysts for hydrodesulfurization (HDS)⁶⁻⁹ hydrodenitrogenation (HDN)¹⁰, hydroprocessing (HPC)¹¹, and hydrogen evolution reaction (HER)¹²⁻²⁰ processes and electrochemical energy storage.^{21, 22} Among transition metal phosphides, nickel phosphides are attracting the greater interest because exhibits superior catalytic activities, especially in the HDS reactions, in comparison with other metal phosphides like Fe₂P, MoP, WP, and Pd₂P₅.²³⁻²⁶ Between nickel phosphides, the hexagonal one, Ni₂P, is the most active as HDS catalyst in comparison with other nickel phosphides such as Ni₁₂P₅, Ni₅P₄ and NiP₂.^{27, 28} Therefore becomes essential the development of methodologies for the selective synthesis of crystal structured control nickel phosphide catalysts. Up today various synthetic routes have been used for the synthesis of Ni₂P nanoparticles in various morphologies, such as solid and hollow nanoparticles^{29, 30} branched nanoparticles and nanorods^{31, 32} and nanowires.³³ Solution phase approaches involves the direct reaction between a nickel and a phosphorous source at elevated temperature and produce particles with very narrow size distribution and discrete sizes. Mainly they are based on the use of inorganic metal salts, metal alkyls or metal carbonyls as metal sources, and alkyl or aryl phosphines³⁴ and phosphine oxides as phosphorous source.^{30, 32, 35-37} These methods are based on the ability of the phosphine and phosphine oxide molecules to act as P atom donors, through their thermal decomposition at temperatures above 250 °C. Furthermore, the use of white phosphorous and, yellow molecular P₄, as a phosphorous source for the synthesis of nickel phosphide nanoparticles has been also reported^{3, 38, 39} and recently Ni₂P nanoparticles in the sub-100 nm size regime were synthesized using a single molecular precursor.⁴⁰ Concerning the synthesis of Ni₂P/graphene nanocomposites the last years a limited number of work appeared in the literature and the most of them focused on the electroactivity of the corresponded materials.⁴¹⁻⁵²

Here we wish to report in the first section of our work an extensive study concerning the synthesis of nickel phosphide nanoparticle in discrete crystal structures introducing a modified phosphidation approach, following by the synthesis of Ni₂P/r-GO nano-hybrids. Both nickel phosphide colloids and composites with r-GO were synthesized in liquid phase, using Ni(acac)₂, as nickel precursor and tri-octylphosphine (TOP), as phosphorous source, in a mixture of aliphatic amines (oleyl amine, tri-octylamine) which seems that play a very important role on the phosphidation process, the size/morphology and the crystal structure of the produced nanoparticles. Finally, the Ni₂P/r-GO hybrid materials were also evaluated as hydrotreating catalysts for the dibenzothiophene HDS in a batch, liquid phase reactor, and reveal a high activity at relatively low temperatures in comparison with similar materials from the literature or commercially available.

EXPERIMENTAL

Materials Synthesis. The nickel phosphide nanoparticles were synthesized following an organometallic approach. In a typical experimental procedure 2 mmol Ni(acac)₂ are dissolved in 20 ml of an oleyl amine/tri-octylamine mixture that containing tri-octylphosphine (TOP), as a phosphorous source, varying the P/Ni²⁺ molar ratio in the 1-18 range. The reaction mixture, after the formation of a clear solution, was heated, under nitrogen atmosphere, at 300 °C and kept at this temperature for 2 h. The colour of the reaction mixture changes from green to dark green and finally turned to black suggesting the nanoparticles formation. Following, the nanoparticles were precipitated, after the temperature solution was cooled down to room temperature, by the addition of ethanol and separated by centrifugation. This procedure was repeated many times to ensure the complete removal of any unreacted organic molecules and reaction by products.

The Ni₂P/r-GO hybrids were synthesized following similar methodology, with sonochemical GO exfoliation before the Ni₂P formation. In particular GO were first dispersed in the aliphatic amines (oleyl amine/tri-octylamine) mixture and probe sonicated in order to exfoliate them, following by the drop-wise addition of the Ni(acac)₂ solution in a similar aliphatic amines mixture which additional includes the phosphorous source, (TOP). Then the reaction mixture was removed from the sonication source and heated up to 300 °C for 2 h under a nitrogen blanket. The products separated first by centrifugation and washed couple of times with a 1/1 ethanol-hexane mixture in order to remove the excess of the organic solvents and reaction by-products, and finally stored in

CHCl₃.

Materials Characterization. All the materials were characterized with powder X-Ray diffraction, using a Siemens D500 diffractometer, with CuK α radiation ($\lambda=1.5418$ Å), while TEM images were collected using a Philips CM20 operated at 200 kV microscope. Raman spectra were recorded with a Labram HR system by HORIBA Scientific, using a laser diode excitation line at 514.5 nm, in the frequency range of 100-3500 cm⁻¹.

Catalytic Evaluation. The catalytic HDS experiments took place in liquid phase, using hexadecane as solvent, and 4,6-dibenzothiophene as sulphur contain molecule, in a batch Parr reactor under H₂, (20 bar), at 300 °C for 4 h. In a typical procedure, 40 mg of the catalyst was dispersed in 50 ml of 1000 ppm dibenzothiophene in n-hexadecane solution. Following, the reactor was purged with He several times, to remove atmospheric air, and the temperature was raised to 300 °C under constant stirring. Then the sealed autoclave was charged with H₂ at the pressure of 20 bar. The overall sulphur content after the HDS reaction was analysed by a sulphur fluorescence analyser (KDS-300).

RESULTS AND DISCUSSION

Colloidal Nickel phosphides. As mentioned, the synthesis of nickel phosphide nanoparticles took place following an organometallic approach which based on the phosphidation using a very common phosphorous source (TOP) in a mixture of aliphatic amines. The nature and the composition of the aliphatic amines mixture it seems that play a very crucial role on the crystal structure, the single-phase nature, the morphology, and the size of the synthesized phosphides nanoparticles. Oleyl amine were extensively studied in the literature as solvent and capping agent, and it is well known that favor the formation of the metal rich Ni₁₂P₅ phase.^{32, 53} The hexagonal Ni₂P phase was observed only under quite high P/Ni²⁺, up to 15, molar ratio³⁴, or under moderate, up to 11.2, P/Ni²⁺ ratio but at higher reaction temperature (up to 350 °C), which enhance the phosphidation process, in order to formed the phosphorous rich phase.^{53, 54}

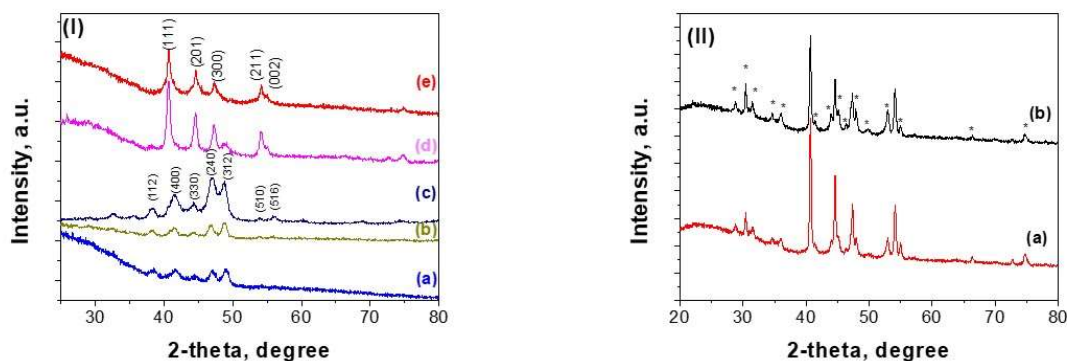


Figure 1. Powder X-ray diffraction patterns of nickel phosphide nanoparticles synthesized in an oleyl amine mono-surfactant medium at 300 °C (I) and 350 °C (II) with different P/Ni²⁺ molar ratio varied from 1 (a), to 3 (b), 9 (c), 12 (d) and 18 (e), for the low temperature reaction, and 1 (a) and 18 (b) for the reaction at 350 °C.

The crystal structure and the phase purity of the nanoparticles were estimated using X-ray diffraction (XRD). In Figure 1, presented the XRD patterns of the as made nickel phosphide nanoparticles synthesized in commercial oleyl amine (80-90 % C18-content) using Ni(acac)₂ and TOP as nickel and phosphorous source respectively. The reaction take place at 300 °C under Ar gas atmosphere for 2 h. The P/Ni²⁺ molecular ratio was varied from 1 to 18 in order to study its effect on the crystal structure of the synthesized nanoparticles.

From the X-ray diffraction patterns it is clear that at very low P/Ni²⁺ molar ratio, in 1-3 range, and low reaction temperature, (300 °C), the nanoparticles have the metal rich tetragonal Ni₁₂P₅ phase, while with the increasing drastically the P/Ni²⁺ molar ratio up to 18, the produced particles reveals the hexagonal phosphorous rich Ni₂P phase. The oleyl amine it was already observed that favours in general the formation of the metal rich phosphides phases^{32, 53}, even under conditions that are more suitable for the formation of the phosphorous rich phases but the mechanism is still remains unknown. In the intermediate P/Ni²⁺ molar ratio values, (in the range 9 to 12), the XRD patterns shows clearly the co-existence of tetragonal and hexagonal crystal structures. More specific when the P/Ni²⁺ ratio is around 9 the dominant phase is the tetragonal one, while with the increasing P/Ni²⁺ molar ratio up to 12, the hexagonal phase became dominant. Finally, at very high, (up to 18), P/Ni²⁺ ratio, value which is among the highest in the literature, the nanoparticles crystallize into the hexagonal Ni₂P crystal structure without any obvious signs of secondary phases. On the

other hand, in the reactions that took place under reflux conditions, near to the oleyl amine boiling point, (348-350 °C), the nanoparticles do not reveal a single phase material, independently the P/Ni²⁺ molar ration, but consist of multiple phosphorous rich phases and more specifically form the Ni₂P and Ni₅P₄. In details, the diffractions at 38.3°, 41.7°, 44.5°, 47.1°, 48.9° 54.1°, 56.1°, 2 θ , (Fig. 1a), are attributed respectively to the (112), (400), (330), (240), (312), (510) and (501) crystal planes of the tetragonal Ni₁₂P₅ phase, (PDF 03-065-1623), while the diffractions at 40.8°, 44.7° 47.4°, 54.4° 2 θ belong to the hexagonal Ni₂P phase (PDF # 74-1385). For the products of the reaction that took place at higher temperature (near to the oleyl amine boiling point), the diffraction peaks which indicated with an asterisk can attributed to the hexagonal Ni₅P₄ phase, (PDF # 03-0652075), while the diffraction at 40.8°, 44.7° 47.4°, 54.4° 2 θ belongs to the hexagonal Ni₂P phase (PDF # 74-1385). Consequently, at high reaction temperature the phosphidation process proceed much faster, and favor the formation of phosphorous rich phases, but with an uncontrollable manner which leads to the formation of mixed phase materials.

Oley amine it is a well-known in the literature coordination agent that bind quite strong on the surface of metallic nanoparticles.⁵⁵⁻⁵⁷ On the other hand, tri-octyl phosphine molecules, mainly because of steric effects originated from the presence of three aliphatic groups, binding weaker with the metallic Ni surface and thus resulting in the need for higher TOP concentration or higher reaction temperature and time, in order to compete the oleyl amine molecules and thus to accelerate the phosphidation procedure for the formation of the phosphide materials. Additionally, when the reaction conditions, and mainly the temperature, favour the phosphidation process, this is happening with a manner that leading to multi-phase phosphorus rich particles.

In terms of morphology it is observableness that the materials were synthesized with high phosphorous concentration, in order to enhance the formation of the hexagonal Ni₂P phase, organized in spherical microparticles, while the particles that synthesized with lower phosphorous concentration and possess the tetragonal Ni₁₂P₅ structure are dense and isolated as evidenced by the TEM images, (presented in Figure 2e), with excellent uniformity, 7.7 nm mean diameter and narrow size distribution (Fig. S1a). Although this organization in larger structures is a common phenomenon for metal nanoparticles,⁵⁸⁻⁶⁰ and oxides nanostructures,⁶¹ it is rarely in phosphides. These hierarchical three-dimensional structures were grown symmetrically in spherical shapes with a narrow size distribution in the sub-micro size regime. The fact that this morphology was not observed in the lower tri-octyl phosphine concentration, shows that the driving force does not

connected with the concentration of the inorganic precursor effect but probably originate from the nature and composition of the organic molecules. The aggregate formation may also be due to van der Waals interactions and needs further investigation but is not in the purpose of the current study.

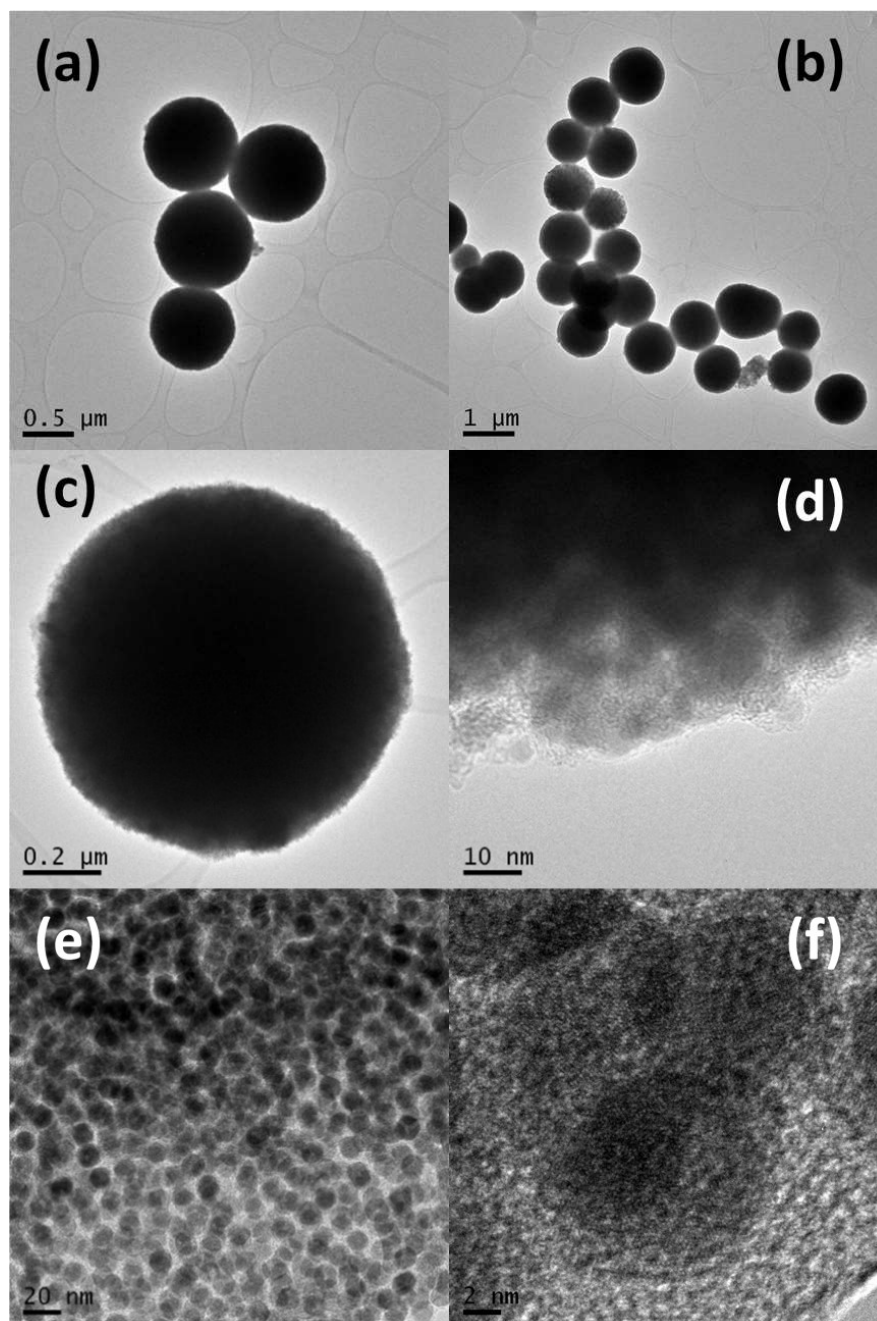


Figure 2. TEM images from the phosphide nanoparticles which were synthesized in oleyl amine with P/Ni²⁺ ratio 18 (a-d) and 1 (e, f).

Aiming to overcome all the above mentioned issues and synthesize the hexagonal structured, phosphorus rich, Ni_2P phase in a controllable way, using as low as possible P/Ni^{2+} ratio, and avoiding high temperatures, we are introducing here an organometallic reaction protocol based on the partial replacement in the reaction mixture of the primary amine, (oleyl amine), which is bind strongly on the metallic surfaces, with a tertiary amine, (tri-octyl amine), which because of the high steric effect, originated form the presence of three alkyl groups, bind on the nanoparticles surface weaker, but “working” similar with oleyl amine as a coordination solvent through the electron pair donor properties.

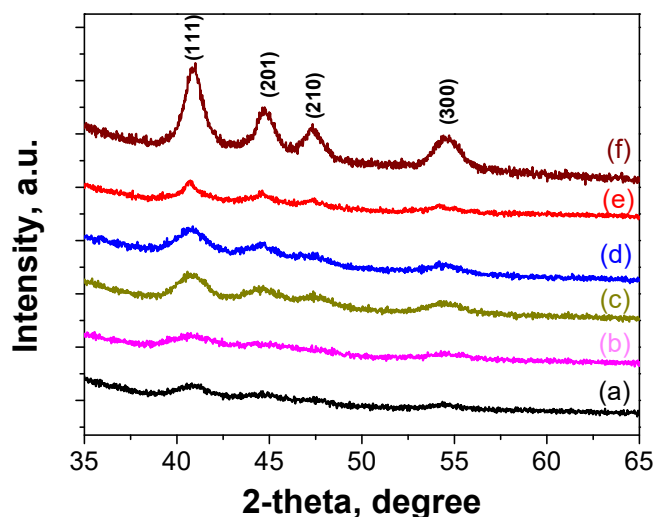


Figure 3. X-ray diffraction patterns of nickel phosphide nanoparticles synthesized in a tri-octylamine/oleyl amine mixture with different v/v ratio, varied from 4/6 (a), 6/4 (b), 7/3 (c), 8/2 (d), to 9/1 (e), and only TOA (f), while the P/Ni^{2+} atomic ratio is 2.8.

Therefore, part of the primary amine (oleyl amine) replaced by an also high boiling point (365 °C) and very stable tertiary amine (tri-octyl amine, TOA), and studied the nickel phosphide synthesis following the same reaction protocol keeping constant the reaction temperature, the reaction volume, and the phosphorous source concentration, ($\text{P}/\text{Ni}^{2+}=2.8$), varying the TOA/oleyl amine volume ratio. The XRD patterns of the corresponded materials (presented in Figure 3), shows that in all cases the synthesized materials possess the hexagonal phosphorus rich Ni_2P phase. In details the diffraction peaks at 40.7° , 44.7° , 47.4° , and 54.4° 2θ can be attributed respectively to the

(111), (201), (210), (300) lattice planes of the hexagonal Ni₂P phase (PDF # 74-1385), while the absence of any other diffraction peaks confirms the single phase nature of the nanoparticles. Concerning the size of the particles it is obvious from the broad width of the diffraction peaks that the particles are quite small and actually in the range of the sub-10 nm in diameter (estimated using Scherrer equation), in contrast with another work, in which the Ni₂P synthesis took place in a low oleyl amine concentration solution in n-octadecene as reaction solvent, the nanoparticles have mean diameter in the range of 10-20 nm and hollow morphology.¹⁹

The nanoparticles size and the morphology were precisely estimated using TEM studies. As the reaction mixture consist form TOA-Oleyl amine with 4/6 v/v ratio the nanoparticles have an elongate morphology with few nanometer thickness (Fig. 4a), while increasing the TOA/oleyl amine volume ratio the nanoparticles becoming uniform, with near spherical shape, and mean diameter which is slightly increase with the increasing of the TOA concentration, but in all the cases remain in the 3-5 nm regime (Fig. 4b-g). There is a noticeable difference when the reaction take place only in TOA. In this case the produced particles were grown in spherical hierarchical three-dimensional structures which consist from 5 nm individual nanoparticles (Fig. 4h-i). Conclusively in the oleyl amine rich environment favor the irregular rod-like nanocrystal formation, while in the tri-octyl amine rich medium, with TOA/oleyl amine v/v ratio 7/3, 8/2 and 9/1, favor the formation of dense, monodispered, with narrow size distribution, spherical nanocrystals with mean diameter in the 4.3 to 5.1 nm size regime. (Fig. S1 b, c, and d). It is obvious that a moderate oleyl amine concentration it is necessary in order to keep the nanoparticles size at low dimensions.

The above findings show distinctly that ultra-small, monodispersed, single phase, *hcp* Ni₂P nanoparticles in the dense solid morphology, can be successfully synthesized in a TOA-Oleyl amine mixture using TOP, as phosphorous source, at relatively low temperatures (300 °C), in the sub-5 nm size regime. Additionally, it is worth to mention that in our approach the solid morphology Ni₂P nanoparticles are synthesized in a relatively low P/Ni²⁺ ratio (2.8), in contrast with the reaction in oleyl amine (P/Ni²⁺=18), and other reported works in which a P/Ni²⁺ molar ratio up to 5.6 is needed in order to synthesize Ni₂P nanoparticles in the solid morphology.⁵³ Thus, the presence of a weaker binding molecule on the surface of the nanoparticles, is very crucial for the phosphidation procedure allowing the crystallization of the nanoparticles into the hexagonal P rich phase. From the mechanistic point of view, the competitive adsorption on the nanoparticles

surface between the tri-octyl amine and tri-octyl phosphine, due to the lower steric inhibition in the tri-octyl phosphine molecule compared to the tri-octyl amine, (P atoms are much bigger than N), favor the phosphine adsorption and thus accelerate the phosphidation process.

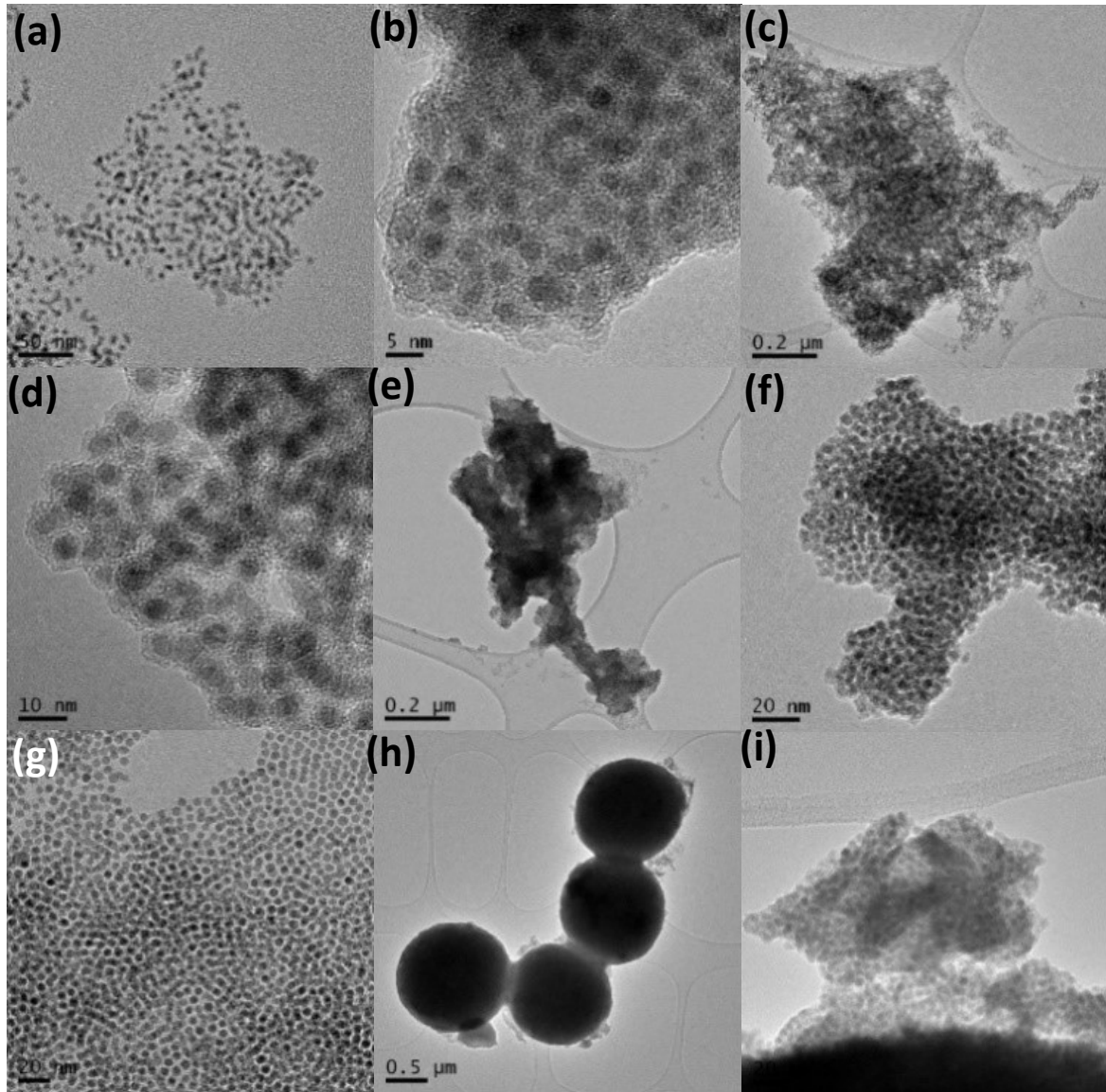


Figure 4. TEM images of Ni₂P nanoparticles synthesized in TOA/Oleyl amine mixture with 4/6 (a), 6/4 (b), 7/3 (c, d), 8/2 (e, f), 9/1 (g) and 10/0 (h, i) v/v ratio.

Ni₂P decorated r-GO. As we already mentioned in the introduction section Ni₂P/graphene nanocomposites have been attracted scientific interest in the last years and the majority of the

research works focused on the electroactivity of the materials either for electrocatalytic or energy storage applications. Following a quite similar synthetic protocol, Lu et al. reported the synthesis of hollow Ni₂P nanoparticles covered by a graphitic layer that coming from the oleyl amine pyrolytic decomposition.⁶² In a recent work the transition metal phosphide/r-GO composites synthesized starting from a metal hydroxide/GO composite material following by a solid state phosphidation at 300 °C and tested for hydrogen evolution reactions (HER).⁴¹ Yolk-shell like Ni₂P/Graphene were synthesized using a solid state procedure and tested for Li and Na ions storage.⁵⁰ The Ni₂P nanoparticles are in the size range of few decades of nanometers with quite broad size distribution.

Utilizing the previously reported findings Ni₂P decorated r-GO were synthesized in liquid phase and tested as catalysts for the dibenzothiophene HSD reaction. In this case the chemical nature of the reaction mixture plays a more complex role. TOA/oleyl amine favor the low temperature phosphidation process and the selective formation of the hexagonal Ni₂P phase, and at the same time both the amine molecules participate into the chemical exfoliation and reduction of the GO⁶³⁻⁶⁵, while the TOP molecules were also contribute to the GO reduction⁶⁵ and serve as P source.

The crystal structure and the morphology of the Ni₂P/r-GO nano-hybrids, were determined by XRD, Raman spectroscopy, and TEM studies. As shown in the powder XRD, in Figure 5(I), all the diffraction peaks correspond to the hexagonal Ni₂P phase, (PDF # 074-1385), while the broad diffraction at 23.9° 2θ, corresponds to the (002) short range order in stacked r-GO sheets. The Raman spectra of Ni₂P/r-GO nano-hybrids exhibits both the characteristic G and D-bands at 1579 and 1347 cm⁻¹ respectively. The G-band at 1579 cm⁻¹, which is associated with sp² hybridized carbon atoms, is asymmetric and shifted near the relevant peak of graphite which is positioned at ~1580 cm⁻¹, indicating the successful removal of the most oxygen-containing groups and the aromatic ring restoration. The asymmetric nature of the G-band peak is due to the presence of a small amount of pristine GO (which reveals the G-band at 1600 cm⁻¹) or less reduced GO. In our case it is clear that the dominant peak is shifted at the lower wavenumbers (around 1579 cm⁻¹) and combined with the I_D/I_G ratio, which is varied from 1.02 to 1.08, we are able to support the successful GO reduction.

The increase of the I_D/I_G was originated by the increase of the sp² domains, upon reduction, within the initial GO sheets and as a decrease in the average size.^{66, 67} Furthermore, while GO does not have significant peaks in the 2D region,^{68, 69} a broad peak arises at 2689 cm⁻¹ in the Raman spectra.

This is ascribed to the 2D vibrational mode (overtone of the D peak).^{70, 71} According to the literature, the red shift of G-band, the intensity of the 2D peak as well as its shift below 2700 cm^{-1} are clear evidence of the r-GO presence with a few layers formation.⁷⁰

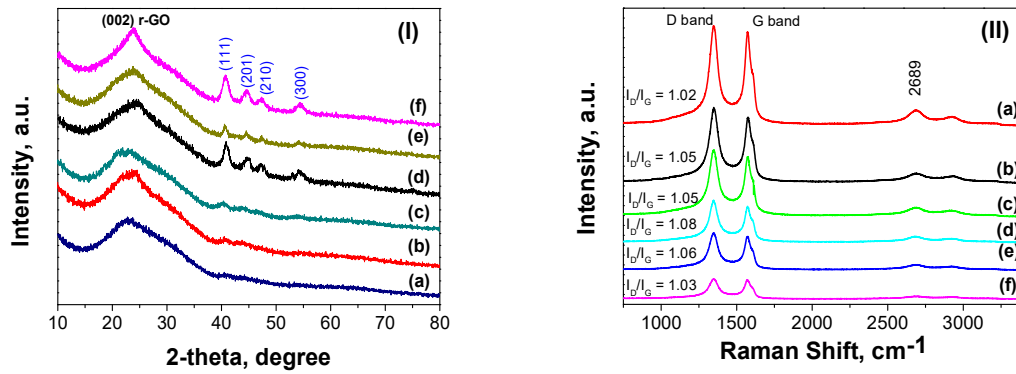


Figure 5. X-ray diffraction patterns (I) and Raman spectra (II) of $\text{Ni}_2\text{P}/\text{r-GO}$ nano-hybrids with 5 (a), 10 (b), 25 (c), 40 (d), 50 (e), and 75 (f) wt. % Ni_2P nominal loading.

The TEM images of $\text{Ni}_2\text{P}/\text{r-GO}$ nano-hybrids, with different Ni_2P loadings, were presented in Figure 6. In most of the cases uniform, monodispersed Ni_2P nanoparticles anchored on the r-GO surface leading to the formation of a more or less dense monolayer of Ni_2P without the presence of isolated nanoparticles which doesn't connected with the r-GO surface. The only exception is the case of the higher metal phosphide loading, in which we can clear observe the presence of a monolayer covering of the r-GO surface with nanoparticles and the presence of not anchored nanoparticles that forms self-assembly superlattices by themselves. At low magnification images is revealed the micron-sized nature of the r-GO sheets. The phosphide nanoparticles are spherical with an average diameter in the sub 5 nm size regime independently the nominal loading. The only difference is the r-GO surface coverage. Concluding, from the TEM observations it seems that our methodology working similarly in a wide range of metal phosphide loading, producing uniformly anchored Ni_2P nanoparticles on the r-GO surface.

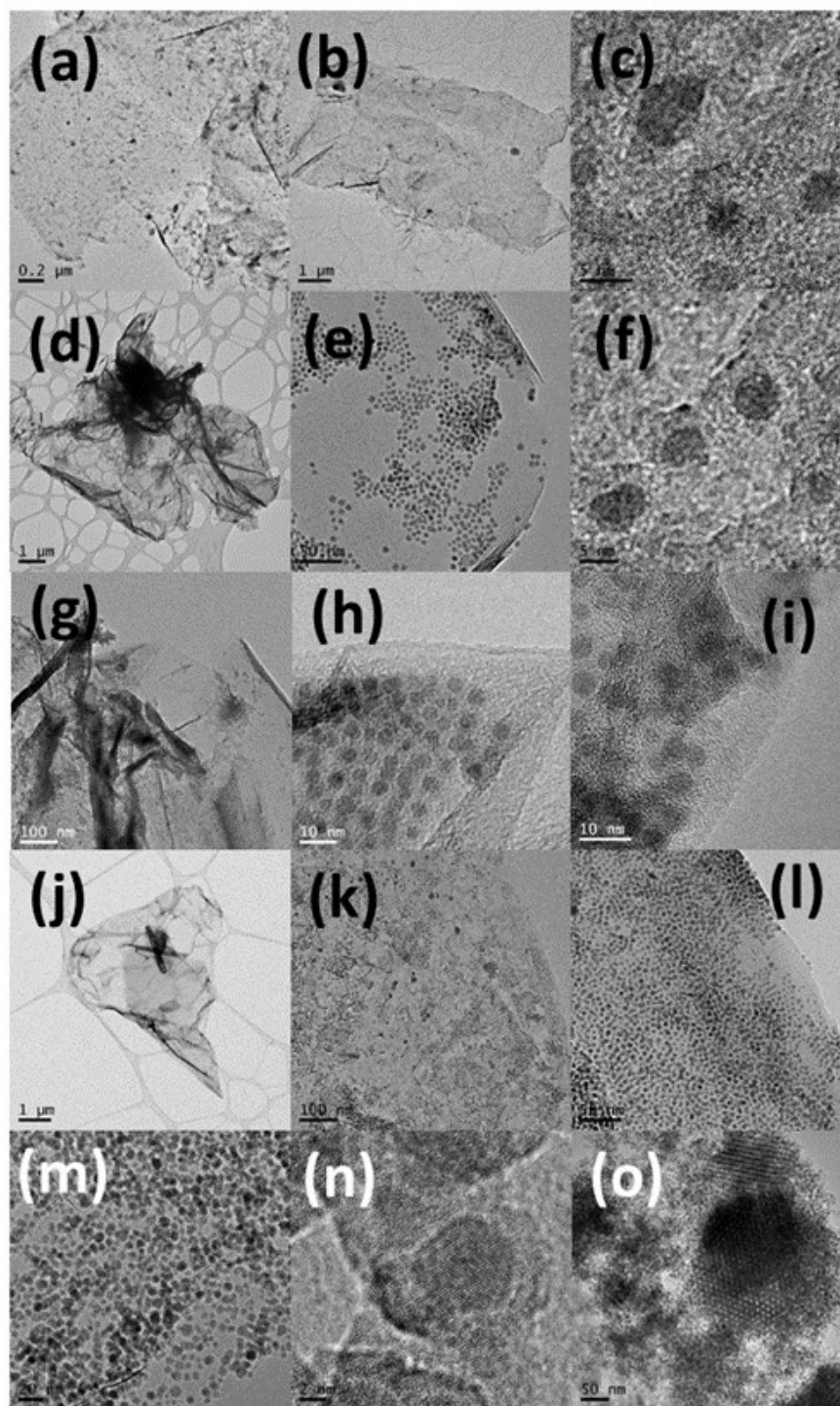


Figure 6. TEM images of Ni₂P/r-GO nano-hybrids with 10 (a-c), 25 (d-f), 40 (g-i), 50 (j-l) and 75 (m-o) wt. % nominal metal phosphide loading.

The Ni₂P/r-GO nanocatalysts were evaluated for the hydrodesulfurization (HDS) of dibenzothiophene (DBT). The HDS reaction took place in a liquid phase batch reactor at 300 °C, using hexadecane as solvent, under 20 bar H₂ pressure, using DBT as sulfur source molecule with 1000 ppm concentration, for 2 h reaction time. For comparison commercially available Ni₂P (Sigma-Aldrich) and MoS₂, (Sigma-Aldrich), which is the most studied and the industrial HDS catalyst, were also tested under the same reaction conditions. The DBT conversion and reaction rates, over different catalytic systems are presented in Figure 7. The DBT conversion is in the range of 10 % for the commercial bulk MoS₂ and almost negligible over commercial Ni₂P (Nickel phosphide, -100 mesh, 98%, Sigma Aldrich) and r-GO, while concerning the Ni₂P/r-GO nanocatalysts the DBT conversion increasing with the increasing of the Ni₂P loading and reach 44 % over Ni₂P/r-GO nanocatalysts with 50 wt. % metal phosphide loading, while for the high dense Ni₂P/r-GO sample decreasing down to 20 %. This behavior can be attributed to the presence of a large nanoparticles population which are not anchoring on the r-GO surface and suffer from sintering and agglomeration effects. From the stability point of view the reaction rate is constant after 2 cycles of HDS for the low Ni₂P loading, while remain in the same level for the 25 and 50 % Ni₂P loading. In the case of 75 % Ni₂P loading the reaction rate decreased dramatically between first, second and third cycle (see ESI section Fig.S2). TEM studies for the materials after the HDS cycles showing that the nanoparticles remain isolated on the r-GO surface, without sintering signs even for the 50 % Ni₂P/r-GO material (see ESI section Figure S3).

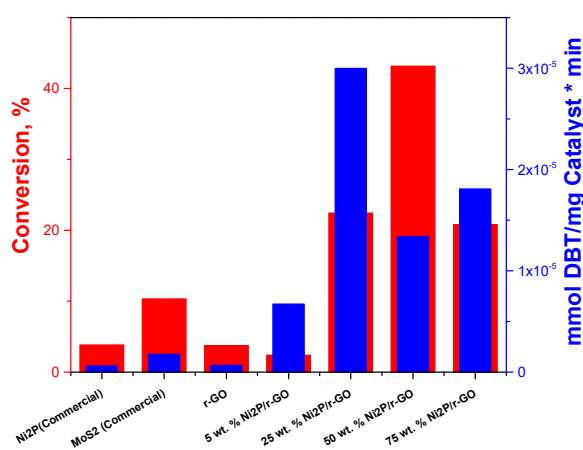


Figure 7. Dibenzothiophene HDS conversion and reaction rate over different catalyst type.

In comparison with the literature the DBT conversion over 10 wt. % supported Ni₂P/SiO₂ is less than 10% for 5, 10 and 15 nm Ni₂P nanoparticles, while for 10 nm Ni₂P²⁴ and Pd₃P₂²⁶ nanoparticles in a core/shell morphology with SiO₂ the DBT conversion at 300 °C is in the range of 5 and 10 % respectively. At 310 °C the DBT conversion can reach 80 % over 20 wt. % Ni₂P on MCM-41 while at 350 °C the conversion is almost 100 %, ⁸ while over Ni₂P/TiO₂-Al₂O₃ the DBT conversion is around 60 % at 310 °C for 3h time on stream.^{72, 73} In all the above studies the reaction take place in a fixed bed continues flow reactor in the gas phase under 30 bar pressure, in contrast with our case that the HDS reaction took place in the liquid phase under batch conditions and 20 bar hydrogen pressure. Independently of the loading and the Ni₂P nanoparticles size it is clear from the data that the DBT conversion is quite high (in the range of 50 %) for reaction temperatures and H₂ pressure higher than 300 °C and 20 bars respectively. In our case, in accordance with our Health, Safety and Environment (HSE) regulations we weren't able to exceed 300 °C and 20 bar H₂ pressure. In general, although the reaction rate constant, according to the Langmuir-Hinshelwood kinetic model, is independent of the reaction solvent the DBT/solvent adsorption constants decrease in the order heptane (gas phase reaction) to hexadecane (liquid phase reaction) due to the competitive adsorption between the DBT and the solvent for the catalytic active sites.⁷⁴ Additionally, the produced H₂S in a batch reactions may also inhibit the dibenzothiophene HDS. Taking into account all the above remarks, including diffusion limitations and competitive adsorption in liquid phase in contrast with the gas phase, we can assume that the presented in the current work Ni₂P/r-GO hybrids are excellent hydro-treating catalyst. Work is on progress for the effect of partial Ni substitution with Co and/or Fe and the formation of a bimetallic or ternary metal phosphide/r-GO composite materials. Preliminary results, presented in Figure S4 in the supplementary section, shows that the developed here phosphidation approach works sufficient for the synthesis of bimetallic Ni-Co phosphides.

CONCLUSIONS

Summarizing we have developed a facile organic phase methodology for the synthesis of ultra-fine Ni₂P nanoparticles by partial replacement of one the most commonly used organic capping agents, oleyl amine, by a tertiary organic amine, tri-octyl amine. The partial primary amine replacement accelerates the phosphidation process due to their steric effect differences, allowing

the formation of the phosphorus rich hexagonal phase Ni₂P nanoparticles at lower temperature, in dense form, and ultra-small sizes with narrow size distribution. Furthermore, the methodology allows the in-situ reduction of graphene oxide (GO) and Ni₂P nanoparticles formation, leading to the formation of Ni₂P/r-GO nano-hybrids. The Ni₂P/r-GO, nano-hybrid materials, were tested as hydrotreating catalysts for the dibenzothiophene hydrodesulfurization and appear, (taking into account that the reaction took place in liquid phase, where competitive adsorptions and diffusion phenomena are quite determinant), to be very active and stable, under the investigated conditions and it turns out that the r-GO can be an excellent alternative, to the inorganic ones, catalysts support for hydrotreating reactions.

ASSOCIATED CONTENT

Supporting Information

In the Supporting Information section were presented the size distribution histograms, additional TEM images of the materials after the HDS reaction, the catalytic activity after the first cycle and preliminary results for the synthesis of bimetallic NiCo phosphides following the presented here chemical methodology.

AUTHOR INFORMATION

Corresponding Authors

* Vasileios Tzitzios, e-mail address: v.tzitzios@inn.demokritos.gr, and Saeed Alhassan, e-mail address: saeed.alkhazraji@ku.ac.ae

ORCID

Vasileios Tzitzios: <https://orcid.org/0000-0002-5687-081X>

Vishnu Pillai: <https://orcid.org/0000-0003-3293-8303>

Marios Katsiotis: <https://orcid.org/0000-0002-9104-584X>

Dimitrios Gournis: <https://orcid.org/0000-0003-4256-8190>

Michael A Karakassides: <http://orcid.org/0000-0003-4344-0375>

Saeed Alhassan: <https://orcid.org/0000-0002-5148-3255>

REFERENCES

1. Carenco, S.; Portehault, D.; Boissiere, C.; Mezailles, N.; Sanchez, C., Nanoscaled metal borides and phosphides: recent developments and perspectives. *Chemical reviews* **2013**, *113* (10), 7981-8065.
2. Shi, Y.; Zhang, B., Recent advances in transition metal phosphide nanomaterials: synthesis and applications in hydrogen evolution reaction. *Chemical Society Reviews* **2016**, *45* (6), 1529-1541.
3. Carenco, S.; Le Goff, X. F.; Shi, J.; Roiban, L.; Ersen, O.; Boissière, C.; Sanchez, C.; Mézailles, N., Magnetic Core– Shell Nanoparticles from Nanoscale-Induced Phase Segregation. *Chemistry of Materials* **2011**, *23* (8), 2270-2277.
4. Miao, S.; Hickey, S. G.; Rellinghaus, B.; Waurisch, C.; Eychmüller, A., Synthesis and characterization of cadmium phosphide quantum dots emitting in the visible red to near-infrared. *Journal of the American Chemical Society* **2010**, *132* (16), 5613-5615.
5. Hitihami-Mudiyanselage, A.; Arachchige, M. P.; Seda, T.; Lawes, G.; Brock, S. L., Synthesis and Characterization of Discrete Fe_xNi_{2-x}P Nanocrystals (0 < x < 2): Compositional Effects on Magnetic Properties. *Chemistry of Materials* **2015**, *27* (19), 6592-6600.
6. Burns, A. W.; Gaudette, A. F.; Bussell, M. E., Hydrodesulfurization properties of cobalt–nickel phosphide catalysts: Ni-rich materials are highly active. *Journal of Catalysis* **2008**, *260* (2), 262-269.
7. Oyama, S. T.; Zhao, H.; Freund, H.-J.; Asakura, K.; Włodarczyk, R.; Sierka, M., Unprecedented selectivity to the direct desulfurization (DDS) pathway in a highly active FeNi bimetallic phosphide catalyst. *Journal of catalysis* **2012**, *285* (1), 1-5.
8. Guan, Q.; Cheng, X.; Li, R.; Li, W., A feasible approach to the synthesis of nickel phosphide for hydrodesulfurization. *Journal of catalysis* **2013**, *299*, 1-9.
9. Fu, W.; Zhang, L.; Wu, D.; Yu, Q.; Tang, T.; Tang, T., Mesoporous zeolite ZSM-5 supported Ni₂P catalysts with high activity in the hydrogenation of phenanthrene and 4, 6-dimethyldibenzothiophene. *Industrial & Engineering Chemistry Research* **2016**, *55* (26), 7085-7095.
10. Badari, C. A.; Lónyi, F.; Drotár, E.; Kaszonyi, A.; Valyon, J., A study of the hydrodenitrogenation of propylamine over supported nickel phosphide catalysts using amorphous and nanostructured silica supports. *Applied Catalysis B: Environmental* **2015**, *164*, 48-60.
11. Li, R.; Guan, Q.; Wei, R.; Yang, S.; Shu, Z.; Dong, Y.; Chen, J.; Li, W., A potential regularity for enhancing the hydrogenation properties of Ni₂P. *The Journal of Physical Chemistry C* **2015**, *119* (5), 2557-2565.
12. Callejas, J. F.; Read, C. G.; Roske, C. W.; Lewis, N. S.; Schaak, R. E., Synthesis, characterization, and properties of metal phosphide catalysts for the hydrogen-evolution reaction. *Chemistry of Materials* **2016**, *28* (17), 6017-6044.
13. Popczun, E. J.; McKone, J. R.; Read, C. G.; Biacchi, A. J.; Wiltout, A. M.; Lewis, N. S.; Schaak, R. E., Nanostructured nickel phosphide as an electrocatalyst for the hydrogen evolution reaction. *Journal of the American Chemical Society* **2013**, *135* (25), 9267-9270.
14. Callejas, J. F.; McEnaney, J. M.; Read, C. G.; Crompton, J. C.; Biacchi, A. J.; Popczun, E. J.; Gordon, T. R.; Lewis, N. S.; Schaak, R. E., Electrocatalytic and photocatalytic hydrogen production from acidic and neutral-pH aqueous solutions using iron phosphide nanoparticles. *ACS nano* **2014**, *8* (11), 11101-11107.

15. McEnaney, J. M.; Crompton, J. C.; Callejas, J. F.; Popczun, E. J.; Biacchi, A. J.; Lewis, N. S.; Schaak, R. E., Amorphous molybdenum phosphide nanoparticles for electrocatalytic hydrogen evolution. *Chemistry of Materials* **2014**, *26* (16), 4826-4831.
16. McEnaney, J. M.; Crompton, J. C.; Callejas, J. F.; Popczun, E. J.; Read, C. G.; Lewis, N. S.; Schaak, R. E., Electrocatalytic hydrogen evolution using amorphous tungsten phosphide nanoparticles. *Chemical Communications* **2014**, *50* (75), 11026-11028.
17. Popczun, E. J.; Read, C. G.; Roske, C. W.; Lewis, N. S.; Schaak, R. E., Highly active electrocatalysis of the hydrogen evolution reaction by cobalt phosphide nanoparticles. *Angewandte Chemie International Edition* **2014**, *53* (21), 5427-5430.
18. Xiao, P.; Sk, M. A.; Thia, L.; Ge, X.; Lim, R. J.; Wang, J.-Y.; Lim, K. H.; Wang, X., Molybdenum phosphide as an efficient electrocatalyst for the hydrogen evolution reaction. *Energy & Environmental Science* **2014**, *7* (8), 2624-2629.
19. Pan, Y.; Liu, Y.; Zhao, J.; Yang, K.; Liang, J.; Liu, D.; Hu, W.; Liu, D.; Liu, Y.; Liu, C., Monodispersed nickel phosphide nanocrystals with different phases: synthesis, characterization and electrocatalytic properties for hydrogen evolution. *Journal of Materials Chemistry A* **2015**, *3* (4), 1656-1665.
20. Kucernak, A. R.; Sundaram, V. N. N., Nickel phosphide: the effect of phosphorus content on hydrogen evolution activity and corrosion resistance in acidic medium. *Journal of Materials Chemistry A* **2014**, *2* (41), 17435-17445.
21. Wang, X.; Kim, H.-M.; Xiao, Y.; Sun, Y.-K., Nanostructured metal phosphide-based materials for electrochemical energy storage. *Journal of Materials Chemistry A* **2016**, *4* (39), 14915-14931.
22. Lu, Y.; Tu, J.; Xiang, J.; Wang, X.; Zhang, J.; Mai, Y.; Mao, S., Improved electrochemical performance of self-assembled hierarchical nanostructured nickel phosphide as a negative electrode for lithium ion batteries. *The Journal of Physical Chemistry C* **2011**, *115* (48), 23760-23767.
23. Korányi, T. I., Phosphorus promotion of Ni (Co)-containing Mo-free catalysts in thiophene hydrodesulfurization. *Applied Catalysis A: General* **2003**, *239* (1-2), 253-267.
24. Layan Savithra, G. H.; Muthuswamy, E.; Bowker, R. H.; Carrillo, B. A.; Bussell, M. E.; Brock, S. L., Rational design of nickel phosphide hydrodesulfurization catalysts: controlling particle size and preventing sintering. *Chemistry of Materials* **2013**, *25* (6), 825-833.
25. Rodriguez, J. A.; Kim, J.-Y.; Hanson, J. C.; Sawhill, S. J.; Bussell, M. E., Physical and chemical properties of MoP, Ni₂P, and MoNiP hydrodesulfurization catalysts: Time-resolved X-ray diffraction, density functional, and hydrodesulfurization activity studies. *The Journal of Physical Chemistry B* **2003**, *107* (26), 6276-6285.
26. Layan Savithra, G. H.; Bowker, R. H.; Carrillo, B. A.; Bussell, M. E.; Brock, S. L., Mesoporous matrix encapsulation for the synthesis of monodisperse Pd₃P₂ nanoparticle hydrodesulfurization catalysts. *ACS applied materials & interfaces* **2013**, *5* (12), 5403-5407.
27. Shu, Y.; Oyama, S. T., A new type of nonsulfide hydrotreating catalyst: nickel phosphide on carbon. *Chemical communications* **2005**, (9), 1143-1145.
28. Ochs, D.; Dieckhoff, S.; Cord, B., Characterization of hard disk substrates (NiP/Al, glass) using XPS. *Surface and Interface Analysis: An International Journal devoted to the development and application of techniques for the analysis of surfaces, interfaces and thin films* **2000**, *30* (1), 12-15.
29. Chiang, R.-K.; Chiang, R.-T., Formation of hollow Ni₂P nanoparticles based on the nanoscale Kirkendall effect. *Inorganic chemistry* **2007**, *46* (2), 369-371.

30. Henkes, A. E.; Vasquez, Y.; Schaak, R. E., Converting metals into phosphides: a general strategy for the synthesis of metal phosphide nanocrystals. *Journal of the American Chemical Society* **2007**, *129* (7), 1896-1897.
31. Sarac, M. F.; Wu, W.-C.; Tracy, J. B., Control of Branching in $\text{Ni}_3\text{C}_{1-x}$ Nanoparticles and Their Conversion into Ni_{12}P_5 Nanoparticles. *Chemistry of Materials* **2014**, *26* (10), 3057-3064.
32. Park, J.; Koo, B.; Yoon, K. Y.; Hwang, Y.; Kang, M.; Park, J.-G.; Hyeon, T., Generalized synthesis of metal phosphide nanorods via thermal decomposition of continuously delivered metal– phosphine complexes using a syringe pump. *Journal of the American Chemical Society* **2005**, *127* (23), 8433-8440.
33. Lu, Y.; Tu, J.-p.; Xiong, Q.-q.; Qiao, Y.-q.; Wang, X.-l.; Gu, C.-d.; Mao, S. X., Synthesis of dinickel phosphide (Ni_2P) for fast lithium-ion transportation: a new class of nanowires with exceptionally improved electrochemical performance as a negative electrode. *RSC advances* **2012**, *2* (8), 3430-3436.
34. Bateer, B.; Wang, X.; Tian, C.; Xie, Y.; Pan, K.; Ping, W.; Fu, H., Ni_2P nanocrystals coated on carbon nanotubes as enhanced lightweight electromagnetic wave absorbers. *Carbon* **2020**, *161*, 51-61.
35. Qian, C.; Kim, F.; Ma, L.; Tsui, F.; Yang, P.; Liu, J., Solution-phase synthesis of single-crystalline iron phosphide nanorods/nanowires. *Journal of the American Chemical Society* **2004**, *126* (4), 1195-1198.
36. Henkes, A. E.; Schaak, R. E., Trioctylphosphine: a general phosphorus source for the low-temperature conversion of metals into metal phosphides. *Chemistry of materials* **2007**, *19* (17), 4234-4242.
37. Andaraarachchi, H. P.; Thompson, M. J.; White, M. A.; Fan, H.-J.; Vela, J., Phase-programmed nanofabrication: Effect of organophosphite precursor reactivity on the evolution of nickel and nickel phosphide nanocrystals. *Chemistry of Materials* **2015**, *27* (23), 8021-8031.
38. Carenco, S.; Resa, I.; Le Goff, X.; Le Floch, P.; Mézailles, N., White phosphorus as single source of “P” in the synthesis of nickel phosphide. *Chemical communications* **2008**, (22), 2568-2570.
39. Barry, B. M.; Gillan, E. G., Low-temperature solvothermal synthesis of phosphorus-rich transition-metal phosphides. *Chemistry of Materials* **2008**, *20* (8), 2618-2620.
40. Pan, Y.; Liu, Y.; Liu, C., An efficient method for the synthesis of nickel phosphide nanocrystals via thermal decomposition of single-source precursors. *Rsc Advances* **2015**, *5* (16), 11952-11959.
41. Li, J.; Yan, M.; Zhou, X.; Huang, Z. Q.; Xia, Z.; Chang, C. R.; Ma, Y.; Qu, Y., Mechanistic insights on ternary $\text{Ni}_{2-x}\text{Co}_x\text{P}$ for hydrogen evolution and their hybrids with graphene as highly efficient and robust catalysts for overall water splitting. *Advanced Functional Materials* **2016**, *26* (37), 6785-6796.
42. Tian, B.; Li, Z.; Zhen, W.; Lu, G., Uniformly sized (112) facet Co_2P on graphene for highly effective photocatalytic hydrogen evolution. *The Journal of Physical Chemistry C* **2016**, *120* (12), 6409-6415.
43. Han, A.; Jin, S.; Chen, H.; Ji, H.; Sun, Z.; Du, P., A robust hydrogen evolution catalyst based on crystalline nickel phosphide nanoflakes on three-dimensional graphene/nickel foam: high performance for electrocatalytic hydrogen production from pH 0–14. *Journal of Materials Chemistry A* **2015**, *3* (5), 1941-1946.

44. Lu, Y.; Wang, X.; Ge, X.; Zhao, X.; Wang, T.; Huang, S.; Gu, C.; Tu, J.; Mao, S., Graphene-wrapped Ni₂P materials: a 3D porous architecture with improved electrochemical performance. *Journal of Solid State Electrochemistry* **2014**, *18* (8), 2245-2253.
45. An, C.; Wang, Y.; Wang, Y.; Liu, G.; Li, L.; Qiu, F.; Xu, Y.; Jiao, L.; Yuan, H., Facile synthesis and superior supercapacitor performances of Ni₂P/rGO nanoparticles. *RSC advances* **2013**, *3* (14), 4628-4633.
46. Lu, Y.; Wang, X.; Mai, Y.; Xiang, J.; Zhang, H.; Li, L.; Gu, C.; Tu, J.; Mao, S. X., Ni₂P/graphene sheets as anode materials with enhanced electrochemical properties versus lithium. *The Journal of Physical Chemistry C* **2012**, *116* (42), 22217-22225.
47. Du, W.; Wei, S.; Zhou, K.; Guo, J.; Pang, H.; Qian, X., One-step synthesis and graphene-modification to achieve nickel phosphide nanoparticles with electrochemical properties suitable for supercapacitors. *Materials Research Bulletin* **2015**, *61*, 333-339.
48. Zhang, G.; Liu, Z.; Xiao, Z.; Huang, J.; Li, Q.; Wang, Y.; Sun, D., Ni₂P-Graphite Nanoplatelets Supported Au-Pd Core-Shell Nanoparticles with Superior Electrochemical Properties. *The Journal of Physical Chemistry C* **2015**, *119* (19), 10469-10477.
49. Bai, Y.; Zhang, H.; Fang, L.; Liu, L.; Qiu, H.; Wang, Y., Novel peapod array of Ni₂P@graphitized carbon fiber composites growing on Ti substrate: a superior material for Li-ion batteries and the hydrogen evolution reaction. *Journal of Materials Chemistry A* **2015**, *3* (10), 5434-5441.
50. Wu, C.; Kopold, P.; van Aken, P. A.; Maier, J.; Yu, Y., High Performance Graphene/Ni₂P Hybrid Anodes for Lithium and Sodium Storage through 3D Yolk-Shell-Like Nanostructural Design. *Advanced materials* **2017**, *29* (3), 1604015.
51. Parveen, N.; Hilal, M.; Han, J. I., Newly Design Porous/Sponge Red Phosphorus@Graphene and Highly Conductive Ni₂P Electrode for Asymmetric Solid State Supercapacitive Device With Excellent Performance. *Nano-Micro Letters* **2020**, *12* (1), 1-16.
52. Zhang, G.; Xu, Q.; Liu, Y.; Qin, Q.; Zhang, J.; Qi, K.; Chen, J.; Wang, Z.; Zheng, K.; Świerczek, K., Red phosphorus as self-template to hierarchical nanoporous nickel phosphides toward enhanced electrocatalytic activity for oxygen evolution reaction. *Electrochimica Acta* **2020**, *332*, 135500.
53. Muthuswamy, E.; Savithra, G. H. L.; Brock, S. L., Synthetic levers enabling independent control of phase, size, and morphology in nickel phosphide nanoparticles. *ACS nano* **2011**, *5* (3), 2402-2411.
54. Liyanage, D. R.; Danforth, S. J.; Liu, Y.; Bussell, M. E.; Brock, S. L., Simultaneous Control of Composition, Size, and Morphology in Discrete Ni_{2-x}Co_xP Nanoparticles. *Chemistry of Materials* **2015**, *27* (12), 4349-4357.
55. Tzitzios, V.; Niarchos, D.; Gjoka, M.; Boukos, N.; Petridis, D., Synthesis and characterization of 3D CoPt nanostructures. *Journal of the American Chemical Society* **2005**, *127* (40), 13756-13757.
56. Tzitzios, V.; Basina, G.; Gjoka, M.; Alexandrakis, V.; Georgakilas, V.; Niarchos, D.; Boukos, N.; Petridis, D., Chemical synthesis and characterization of hcp Ni nanoparticles. *Nanotechnology* **2006**, *17* (15), 3750.
57. Mourdikoudis, S.; Liz-Marzán, L. M., Oleylamine in nanoparticle synthesis. *Chemistry of Materials* **2013**, *25* (9), 1465-1476.
58. Pelzer, K.; Vidoni, O.; Philippot, K.; Chaudret, B.; Colliere, V., Organometallic Synthesis of Size-Controlled Polycrystalline Ruthenium Nanoparticles in the Presence of Alcohols. *Advanced Functional Materials* **2003**, *13* (2), 118-126.

59. Song, Y.; Yang, Y.; Medforth, C. J.; Pereira, E.; Singh, A. K.; Xu, H.; Jiang, Y.; Brinker, C. J.; van Swol, F.; Shelnett, J. A., Controlled synthesis of 2-D and 3-D dendritic platinum nanostructures. *Journal of the American Chemical Society* **2004**, *126* (2), 635-645.
60. Schmid, G.; Lehnert, A.; Malm, J. O.; Bovin, J. O., Ligand-Stabilized Bimetallic Colloids Identified by HRTEM and EDX. *Angewandte Chemie International Edition in English* **1991**, *30* (7), 874-876.
61. Panagiotopoulos, I.; Alexandrakis, V.; Basina, G.; Pal, S.; Srikanth, H.; Niarchos, D.; Hadjipanayis, G.; and Tzitzios, V. Synthesis and Magnetic Properties of Pure Cubic CoO Nanocrystals and Nanoaggregates. *Crystal Growth and Design* **2009**, *9* (8), 3353-3358.
62. Lu, Y.; Tu, J.-p.; Gu, C.-d.; Wang, X.-l.; Mao, S. X., In situ growth and electrochemical characterization versus lithium of a core/shell-structured Ni₂P@C nanocomposite synthesized by a facile organic-phase strategy. *Journal of Materials Chemistry* **2011**, *21* (44), 17988-17997.
63. Nethravathi, C.; Rajamathi, M., Selective sorption of amines by graphite oxide: Brønsted basicity is the major factor for selectivity. *Carbon* **2020**, *158*, 97-101.
64. Dang, D. K.; Kim, E. J., Solvo thermal-assisted liquid-phase exfoliation of graphite in a mixed solvent of toluene and oleylamine, *Nanoscale Res. Lett.* 2015.
65. Liu, J.; Jeong, H.; Liu, J.; Lee, K.; Park, J.-Y.; Ahn, Y.; Lee, S., Reduction of functionalized graphite oxides by trioctylphosphine in non-polar organic solvents. *Carbon* **2010**, *48* (8), 2282-2289.
66. Lucchese, M. M.; Stavale, F.; Ferreira, E. M.; Vilani, C.; Moutinho, M. V. d. O.; Capaz, R. B.; Achete, C. A.; Jorio, A., Quantifying ion-induced defects and Raman relaxation length in graphene. *Carbon* **2010**, *48* (5), 1592-1597.
67. Tuinstra, F.; Koenig, J. L., Raman spectrum of graphite. *The Journal of chemical physics* **1970**, *53* (3), 1126-1130.
68. Kouloumpis, A.; Spyrou, K.; Dimos, K.; Georgakilas, V.; Rudolf, P.; Gournis, D., A bottom-up approach for the synthesis of highly ordered fullerene-intercalated graphene hybrids. *Frontiers in Materials* **2015**, *2*, 10.
69. Kaniyoor, A.; Ramaprabhu, S., A Raman spectroscopic investigation of graphite oxide derived graphene. *Aip Advances* **2012**, *2* (3), 032183.
70. Ferrari, A. C.; Meyer, J.; Scardaci, V.; Casiraghi, C.; Lazzeri, M.; Mauri, F.; Piscanec, S.; Jiang, D.; Novoselov, K.; Roth, S., Raman spectrum of graphene and graphene layers. *Physical review letters* **2006**, *97* (18), 187401.
71. Kudin, K. N.; Ozbas, B.; Schniepp, H. C.; Prud'Homme, R. K.; Aksay, I. A.; Car, R., Raman spectra of graphite oxide and functionalized graphene sheets. *Nano letters* **2008**, *8* (1), 36-41.
72. Chen, T.; Yang, B.; Li, S.; Wang, K.; Jiang, X.; Zhang, Y.; He, G., Ni₂P catalysts supported on titania-modified alumina for the hydrodesulfurization of dibenzothiophene. *Industrial & engineering chemistry research* **2011**, *50* (19), 11043-11048.
73. Wei, R.; Zhu, Q.; Han, F.; Guan, Q.; Li, W., Comparison of four different synthetic routes of Ni₂P/TiO₂-Al₂O₃ catalysts for hydrodesulfurization of dibenzothiophene. *Rsc Advances* **2015**, *5* (48), 38774-38782.
74. Contreras-Valdez, Z.; Mogica-Betancourt, J. C.; Alvarez-Hernández, A.; Guevara-Lara, A., Solvent effects on dibenzothiophene hydrodesulfurization: Differences between reactions in liquid or gas phase. *Fuel* **2013**, *106*, 519-527.

Graphic for the Table of Content

